A Level Set Approach to Simulating *Xenopus laevis* Tail Regeneration

Zachary Serlin[1], Jason Rife[1] and Michael Levin[2]

[1]Automated Systems and Robotics Laboratory, Tufts University, Medford, MA 02155
[2]Center for Regenerative and Developmental Biology, Tufts University, Medford, MA 02155
Zachary.Serlin@tufts.edu; Jason.Rife@tufts.edu; Michael.Levin@tufts.edu

Abstract

A framework for predictively linking cell-level signaling with larger scale patterning in regeneration and growth has yet to be created within the field of regenerative biology. If this could be achieved, regeneration (controlled cell growth), cancer (uncontrolled cell growth), and birth defects (mispatterning of cell growth) could be more easily understood and manipulated. This paper looks to create a key part of this preliminary framework by using level set methods and a cellular control scheme to predict macroscopic regenerative morphology. This simulation specifically looks at *Xenopus laevis* tail regeneration, and uses three control regimes to collectively mimic biological regeneration. The algorithm shows promise in creating an abstracted model to predict cell patterning on a macroscopic level.

Introduction

If the control of cell growth and tissue patterning can be better understood, cancer (uncontrolled cell growth), birth defects (mispatterning), and organ regeneration (cell growth harnessed toward the repair of complex organs) could be more easily manipulated. While the molecular mechanisms of cellular control are increasingly understood, the field lacks frameworks for predictively linking cell-level signals to large-scale pattern controls. This paper looks to leverage methods from continuum mechanics to provide new tools for modeling the control of cell growth and patterning. To do this, regeneration in tadpole tails is modeled as an iteration between two processes. The first process is a control scheme, which decides where and when tissue should grow or shrink. The second process is a growth model that describes changes in tissue morphology due to cell division, motion, and growth.

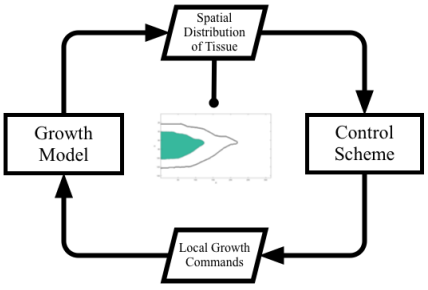

Figure 1: Two-process system model. The control scheme creates local growth commands, which the growth model uses to outputs the spatial distribution of tissue.

One challenge in modeling regeneration and tissue growth is relating the macro (organism) scale to the micro (cell) scale. Traditionally, as the scale of the organism increases, so does the computational expense of modeling its smallest features and interactions. The average human is composed of 37.2 trillion cells – an unrealistic number of cells and interactions to model (Bianconi et al. 2013). Our proposed method is advantageous because it treats tissue as a continuum, blurring the boundaries between individual cells. This approach avoids the problem of managing cells as individual agents, which like marbles on a Chinese checkers board, would need to be shuffled to open spaces to make room for new marbles.

What we describe is the difference between tracking individual agents and tracking the motion of bulk material through a fixed volume of space. Two types of mathematical thinking exist to distinguish these types of phenomena. The first approach is Lagrangian, meaning cells are tracked on an individual basis. Such a method allows cells to operate on their own growth rules and is commonly used in biological growth modeling (Walker et al. 2004; Rejniak and Anderson 2011). Lagrange models often suffer morphologically from internal voids because the individual "cells" cannot directly organize in a manner that preserves contact without overlapping. The second approach is Eulerian, meaning it focuses on the space through which particles move. Eulerian approaches are classically employed in modeling fluid flow and heat transfer (J. A. Sethian 1985; Osher and Sethian 1988). Such methods have not been widely used to model tissue growth and patterning; however, they offer great promise to capture the effects of microscopic phenomena interacting across macroscopic domains.

Our proposed model uses an Eulerian approach based on the level-set method. Level sets use a modified mass balance to describe a moving boundary, such as the interface between an organism and the surrounding medium. Level set methods are used to model crystal growth and combustion, as well as for computer vision and microchip fabrication (Osher and Sethian 1988; J. A. Sethian 1985; J. Sethian 1984; J. A. Sethian, n.d.). Level set methods have also seen some use in biological modeling (C.S. Hogea, Murray, and Sethian, n.d.) although not to our knowledge in a closed-loop feedback scheme for patterned growth as illustrated in Figure 1.

Level set methods use a scalar field to describe a moving boundary. The boundary is at the zero values of the scalar field and motion of the boundary is determined by assigning a speed at each point. The speed function is ultimately what controls the development of the boundary. For this biology-motivated

application, we propose a speed function consisting of three main components: isometric control, patterning control, and smoothing control.

This paper uses level sets to simulate the regeneration of the amputated tail of a *Xenopus laevis* tadpole. *Xenopus* is a simple vertebrate that regenerates its tail until early in its life cycle, through stage 52 or 53 (Suzuki et al. 2006). This makes *Xenopus* ideal for modeling patterning growth, and regeneration in particular, across a macroscopic scale. In this work, we conceptualize regeneration as growth that restores animal morphology back to a "reference" shape. Our particular approach will assume that a global reference map is available and that control laws act by setting growth rate based on the distance of the organism boundary from the reference. In fact, it is not critical as to whether an actual reference "map" might exist in an animal system (Friston et al. 2015) or whether the "map" is an emergent pattern that results from local control decisions (Zhang and Levin 2009; Chernet, Fields, and Levin 2015). On the simulation scale, both mechanisms are functionally equivalent.

In the following sections, this paper will detail methods used to implement the growth model and the control scheme. The paper will then go into detail on the simulation used to assess these models. Finally, we will present results, conclusions, and future work.

Methods

Level Set Analogy

Level set methods were originally created to model combustion and two-phase flow (J. Sethian 1984). A level set can be conceived as a geographic contour map, where each level set is an elevation contour that consists of the set of points at a particular elevation. These contours may change over time if geography changes. By following a particular contour in time, it is possible to model the motion of an interface (e.g. a flame front in combustion or a liquid-gas interface in two-phase flow). The level set equation is directly related to the scalar transport equation. Instead of transporting material however, the level set method transports a scalar distance from the boundary of interest.

To make the geographic analogy more concrete, consider a particular case – a volcanic island rising out of the ocean (Figure 2). In this example, we will track *sea level* over time, as this elevation marks the interface between the island and the ocean. As a volcanic eruption takes place and adds material over the entire island, the island's elevation map will evolve both on the land side (topography) and on the ocean side (bathymetry). The addition of new material will cause the island to grow, such that the sea-level elevation contour pushes outward as shown in Figure 2. Erosion would garner the opposite effect – sharp features would be worn down, shrinking the boundary. In Figure 2, the elevation is denoted by the scalar ϕ. The interface between land and water is denoted by the sea-level contour, with $\phi = 0$.

This geographic concept can be extended to biological modeling. In this paper, we consider a two-dimensional model of the *Xenopus* tail. In our model, the *x* coordinate corresponds to the anterior-posterior direction, the *y* coordinate to the dorsal-ventral direction, and the lateral direction is not modeled. The level set field $\phi(x,y)$ is now used to represent distance away from the outer surface of the organism. The contour that represents the outer surface of the organism is labeled Γ and represents the set of all points where $\phi = 0$. Moving inside the organism, the distance-from-contour is measured as positive and so ϕ is set positive inside the organism. By contrast, ϕ is set negative outside the organism. This mathematical approach lets us track the motion of the outer surface of the organism through space as the organism grows in time. An illustration of this concept is shown in Figure 3, which depicts a section of the *Xenopus* tail. A photo of the *Xenpous* tadpole, in Figure 3(a), shows the tail prior to amputation. The outer tail surface can be identified and used to

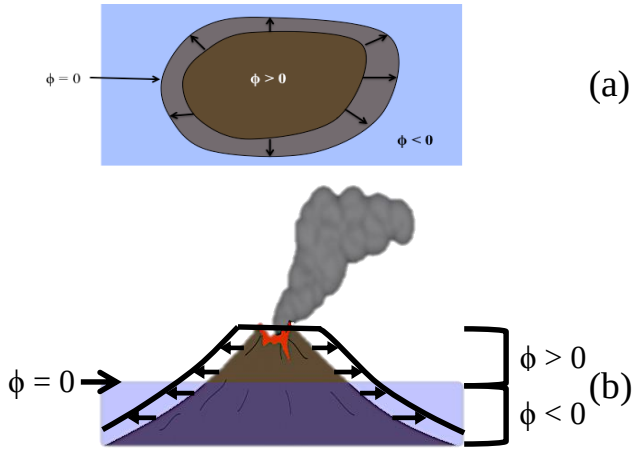

Figure 2: (a) Top view of the volcanic island erupting – arrows indicate boundary movement. (b) Front view of the volcanic island describing the same boundary movement. Elevation above sea level is indicated by the variable ϕ. Addition of volcanic material increases elevation and translates directly to change in island circumference.

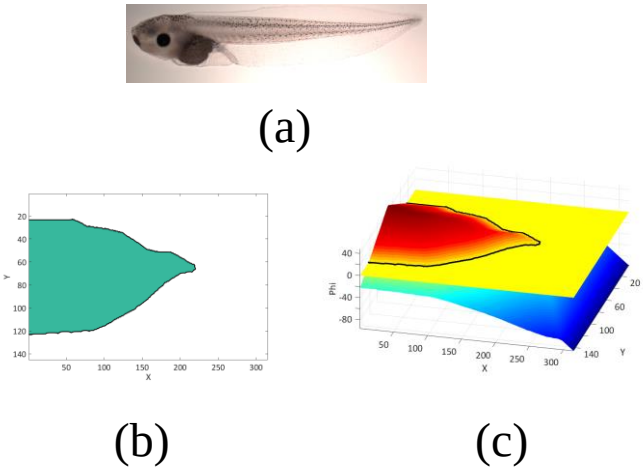

Figure 3: Level Set Scalar Field Derivation (a) *Xenopus laevis* at stage 42. (b) A 2D view of the tail representation. This represents the morphology of the tail and is the zero level set contour of the scalar field. (c) A 3D representation of the level set field. The flat plane is the zero level set. Above that plane represents material inside the body; while, the section below that plane is outside the body. The black line represents the current zero contour.

generate a binary image, as shown in Figure 3(b), where the green region indicates the interior of the organism and the light region indicates the exterior. This tail region can also be viewed as a level set field, shown in three-dimensions in Figure 3(c). The height of the field indicates the distance of each (*x*,*y*) point from the outer surface of the organism.

Growth Model

This section describes the level set equations we used to model organism growth. Begin by identifying the outer surface of the organism in a Cartesian space described by coordinates *x* and *y*. In two-dimensions, the outer surface of the animal is a contour, which we label Γ as shown in Figure 3(b). Now construct a scalar field $\phi(x,y)$ that represents distance from the contour Γ, with values increasing interior to the organism ($\phi > 0$) and decreasing exterior to the organism ($\phi < 0$). In order to represent distance, note that the gradient of this scalar field must be one at all points where the slope of the field is continuous. Slope discontinuities appear only at the center of the field, where points are equidistant from multiple sections of the Γ contour, as illustrated by the ridge that appears along the midline of the tail, as illustrated in Figure 3(c).

To model growth, we evolve the scalar field ϕ over time. As time advances, the level set is propagated using a velocity field **v**(x,y), where the velocity vector is specified at every point in the field. The magnitude *F* of the velocity vector will be set by the control scheme, as described below. As the control scheme transform the scalar field, the outer surface of the organism Γ moves in time, representing organism growth.

The following equation governs the time dynamics of the scalar field $\phi(x,y,t)$.

$$\frac{D}{Dt}\phi = S(x,y,t) \tag{1}$$

Here the full derivative of the scalar ϕ is related to a source term *S*. The source term allows for the production of new material (or the destruction of old material) at every point in the field. Where the source term is zero, there is no change in the total amount of material present; in other words, ϕ is conserved in the absence of a source term. Equation (1) is a classical conservation law from continuum mechanics, as might be used to model the conservation of mass, momentum, or energy (Kundu, Cohen, and David R. Dowling Ph.D. 2011).

The full derivative is linked to velocity **v** through the following equation.

$$\frac{D}{Dt}\phi(x,y,t) = \phi_t + \nabla\phi \cdot \mathbf{v} \tag{2}$$

This equation, obtained from standard calculus using the chain rule, uses the notation ϕ_t to identify the partial derivative of ϕ with respect to time and the notation $\nabla\phi$ to identify its spatial gradient. In this work, ϕ contours are assumed always to move outward in the direction normal to each existing contour. The local unit normal to each contour is defined by the gradient:

$$\mathbf{n} = \frac{\nabla\phi}{\|\nabla\phi\|} \tag{3}$$

The velocity vector can be written in terms of a magnitude term *F* multiplied by this local normal.

$$\mathbf{v} = -F\mathbf{n} \tag{4}$$

The negative sign is introduced here, so that a positive speed *F* corresponds to organism growth (toward lower values of ϕ).

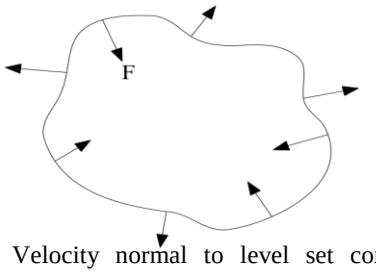

Figure 4: Velocity normal to level set contour. All movement is normal to each point on the contour. Only the magnitude of *F* determines contour movement.

A field in which velocity is locally normal to the contour is shown in Figure 4.

Substituting equation (4) into equation (2) gives

$$\frac{D}{Dt}\phi(x,y,t) = \phi_t - F\|\nabla\phi\| \tag{5}$$

Recalling that the gradient is equal to one at all points where it is defined, the full derivative becomes

$$\frac{D}{Dt}\phi(x,y,t) = \phi_t - F \tag{6}$$

where the gradient $\nabla\phi$ is continuous. To avoid issues with the gradient being undefined at some locations (at cusps and ridges in the ϕ field), the velocity magnitude *F* is restricted to be zero at these locations. Thus, by combining equations (1) and (6), we obtain the following equation to describe the change in the level set field ϕ at each point and at each moment in time.

$$\phi_t = \begin{cases} F + S, & \nabla\phi \; defined \\ S, & elsewhere \end{cases} \tag{7}$$

Because this equation for propagating the ϕ field behaves differently in regions where the gradient is either continuous or not, it is natural to decompose our solution approach into two parts. In the first part of the solution, we update the field at each time step assuming that the source term is negligible. For this step we use a first-order discretization of equation (7).

$$\phi(t+\Delta t) = \begin{cases} \phi(t) + F\Delta t, & \nabla\phi \; defined \\ \phi(t), & elsewhere \end{cases} \tag{8}$$

Assuming a negligible source term is reasonable over short time periods; however, over longer periods neglecting the source term rapidly degrades the assumption that the gradient is unity magnitude (where defined), since a source should exist at peaks and ridges (as in the Volcano example of Figure 2). As such, the source term must be taken into account somehow.

To account for the source term, we use a process called reinitialization (J. A. Sethian 1985; Osher and Sethian 1988; Brakke 2015; Evans and Spruck 1991). Reinitialization serves two purposes; it forces the non-boundary region to have a gradient of one, and it implicitly adds material to the whole field to maintain the field's shape. In particular, we use a process called a narrowband reinitialization (J. A. Sethian, n.d.). The narrowband solution assumes that the location of the zero-contour Γ is predicted accurately. The solution domain is then divided into two regions: a region near the zero-contour (the *interface* region) and the region farther from the zero-contour (the *far field*). Values of ϕ in the interface region are

preserved; values in the far field are replaced by computing the distance of each location from the zero contour. Although this process does not correct the gradient inside the interface region, the far field values effectively introduce a boundary condition that drives the slope in the interface region back toward its correct magnitude (of one). This narrowband approach is numerically robust and has been used extensively in other applications of the level set method (J. A. Sethian, n.d.).

A practical issue is that the approximations introduced by narrow banding can affect the accuracy of the prediction of the zero-contour Γ. A balance must be struck however between giving the zero-contour freedom of movement and constraining the field to a gradient of one. For this reason, reinitialization is not necessarily performed at every time update. In our method, we used a boundary width of 2 pixels on either side of the Γ contour and performed reinitialization at a rate of once per 20 time steps.

In summary, the key idea of the growth model is that a velocity field can be assigned to every point in space, allowing the organism surface Γ to be grown without knowing the precise location of that surface. This property is in turn useful because it permits the simulation of a smooth, continuous boundary using a relatively coarse grid.

Control Scheme

In this section we describe a control law that can be used to in conjunction with the level set methodology to define organism shape during regeneration. The control law defines a velocity field at every point in the simulation domain. As described by equation (4), the velocity is locally normal to contours of constant ϕ. The velocity magnitude *F* is set by the control described in this section. Specifically, *F* is a summation of three terms, which are assumed to act independent of each other. These terms include patterning control *P*, isometric control *I*, and smoothing control *K*. Each term models a distinct aspect of biological growth. It is important to note, however, that the models are phenomenological in nature and are not derived directly from detailed data sets. Taken together, the three terms sum to give *F*.

$$F = P + I + \mathrm{K} \tag{9}$$

All terms in this equation are functions of 2D space and time.

Patterning Control: Patterning control, *P*, is the key term for this paper as it shapes morphology by enabling local growth. The idea is that local cell-level actions may trigger tissue deterioration or growth in a small region (as at the regeneration site or *blastema* in an amputated *Xenopus* tail (King and Newmark 2012)). These local actions are responsible for regeneration and also for shape changes that occur during normal growth. Furthermore, this local activity counteracts disturbances, constantly adding or removing tissue to maintain an appropriate organism shape under varying environmental conditions. In principle, a failure of local patterning might result in uncontrolled growth (i.e. cancer).

In our simulation, we assume that patterning growth is active for cells that are near the organism surface Γ but that are not at a desired location. For simplicity, we use a global reference map ϕ_{ref}, which is scaled to the current width of the simulated tail. From this map, we derive an error *e* at each point in the simulation domain.

$$e(x,y,t) = \phi_{ref}(x,y,t) - \phi(x,y,t) \tag{10}$$

The error for a given element of tissue represents the difference between its desired and actual distance from the organism surface. The error term is limited to a maximum value, e_{max}, to reflect a threshold where the cells are so far from their target that they grow at a maximum rate. In the region near the organism surface, the patterning speed is set to be proportional to the error, modulated by a patterning control gain labeled C_P.

This proportionality is capped, however, to reflect a maximum cellular growth rate, which is slightly faster than nominal, isometric growth. The maximum speed F_{max} is related to the maximum cellular growth rate $C_{GC,max}$.

$$F_{max} = \frac{V_{pat}}{SA} C_{GC,max} \tag{11}$$

Here the variable *SA* represents the surface area (which in 2D is the length of the contour where ϕ = 0). The variable V_{pat} represents the volume of tissue that is active in patterning and is proportional to V_{tot}. The result is that patterning growth is nonzero only in the active region; in this region patterning growth is nominally proportional to error, subject to saturation if the growth rate becomes too large or too small.

$$P = \begin{cases} F_{max}\frac{e}{e_{max}} & |e| < e_{max} \text{ and } 0 < \phi \le d \\ F_{max}\mathrm{sign}(e) & |e| \ge e_{max} \text{ and } 0 < \phi \le d \\ 0 & otherwise \end{cases} \tag{12}$$

Isometric Control: Our simulation uses an isometric control term *I* to allow for growth that is organism wide (as compared to patterning growth which is local). We assume that this growth occurs at the same rate throughout the entire organism, such that the organism maintains its shape when only *I* is active. Isometric growth is, in fact, a nominal behavior for some organisms such as the flatworm. When food resources are plentiful, the flatworm grows uniformly in all directions; when the flatworm is starved it shrinks uniformly in all directions (Lobo, Beane, and Levin 2012). In *Xenopus* tadpoles, by contrast, some changes in shape occur as the organism grows (Love et al. 2013; Suzuki et al. 2006; Chernet, Fields, and Levin 2015), and so nominal growth combines some aspects of isometric control *I* with patterning control *P*.

The isometric control term has a uniform value of C_V everywhere in the simulation domain when the term is active.

$$I = F_V \tag{13}$$

The isometric model represents constant cellular growth with time, meaning the boundary velocity must increase in time (as the volume to surface area ratio increases). To account for this, the growth speed F_v is computed as

$$F_V = \frac{Vtot}{SA} C_{GC,nom} \tag{14}$$

Here V_{tot} represents the total volume of the organism (or in this 2D simulation, the area of the tail). The rate $C_{GC,nom}$ represents the rate of cellular growth (mitosis), which is modeled to be uniform in space . For our simulations we assume that sufficient resources are available to the organism to maintain a nominal growth rate $C_{GC,nom}$ that is constant in time.

Smoothing Control: The final term of the speed function is a smoothing control term K designed to eliminate sharp features (e.g., corners created by amputation) or to eliminate tissue

filaments that might (by random chance) begin to develop as extensions of the organism surface. This term essentially regularizes the organism surface to maintain smoothness. The specific mechanism for performing smoothing is to introduce a perturbation to the growth rate that is proportional to the local curvature κ of the ϕ contours. The constant of proportionality is C_κ.

$$K(x,y,t) = C_\kappa \kappa(x,y,t) \quad (15)$$

This concept for smoothing has been employed in other applications of level set methods, as described by (J. A. Sethian, n.d.; Brakke 2015; Evans and Spruck 1991; Osher and Sethian 1988). In our biological application, the curvature term not only eliminates spurious features; it is meant to prevent the formation of holes and discontinuities that are not represented in the reference map.

By definition, curvature in a level set is the spatial derivative of normal vectors along a contour. The more rapidly the contour changes direction, the higher will be its curvature. Mathematically, curvature can be written

$$\kappa = \nabla \cdot \mathbf{n} \quad (16)$$

where the normal vector **n** is defined by equation (3) above.

Each control regimes can be linked directly to micro scale cell behavior that impacts macro scale morphology. Patterning control begins by considering a maximum growth rate of individual regeneration, multiplies that growth by the number of patterning cells, and then distributes that growth along the growing boundary. Similarly, isometric control begins by considering the natural growth rate of cell division, multiples that growth by the cells in the tail, and distributes this growth over the body boundary by dividing by the surface area of the tail. Smoothing control is not as simply related to cell growth, but instead represents cohesiveness in the cellular matrix by minimizing areas of high curvature or irregularity.

Implementation

Each time step is represented by a single iteration of the main loop shown in Figure 5. In general, the simulation is allowed to run for 15,000 time steps, but this number must be adapted to grid resolution and control coefficients.

The level set ϕ is stored as a two-dimensional array on a Cartesian x-y grid. In this simulation the size of the grid was 301 pixels (anterior-posterior) and 135 pixels (dorsal-ventral). Two extra cells pad the field on each edge to simplify gradient and curvature calculations.

Computing $\|\nabla\phi\|$ (labeled Magnitude of Gradient of Phi block in Figure 5) introduces a potential source of numerical error, as derivative operations amplify numerical errors. Therefore, a weak Gaussian filter was introduced in this block to smooth gradient values. The filter uses a two-dimensional Gaussian kernel with a standard deviation of 0.25.

At each step, the surface of the organism ($\phi = 0$) may lie between cells. No attempt is made to interpolate the actual surface (e.g. red contour shown in Figure 6). Rather, figures in this paper report all cells with $\phi > 0$ as being part of the organism and all cells with $\phi < 0$ as being exterior to the organism.

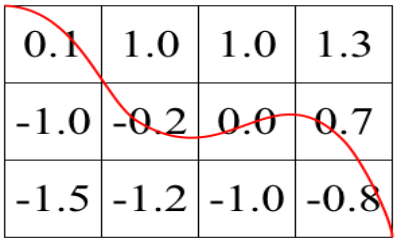

Figure 6: The boundary (red curve) may lie between cell centers, as shown on this grid.

Results of Simulation Verification

A suite of four test cases were simulated in order to verify the basic functionality of the algorithm. The four test cases all considered a simulation domain modeling a stereotypical *Xenopus* tadpole tail. The final tail morphology is derived from Reid et. al. (Reid, Song, and Zhao 2009)and The Normal Table of Xenopus laevis (Faber and Nieuwkoop 1967). The four tests include (a) no growth, (b) patterning-based regeneration following amputation, (c) nominal isometric growth, and (d) nominal isometric growth and simultaneous regeneration following amputation. These test cases were selected respectively to examine algorithm stability, performance of patterning control (in isolation), performance of isometric control (in isolation), and performance of combined control terms.

Patterning and isometric control parameters are derived from experimental regeneration data. All four test cases have (unless otherwise noted) $C_{Gc,nom}$ = 0.00075, C_κ = 0.001, C_p = 0.02, d = 3, e_{max} = 10, $C_{Gc,max}$ = 0.1, 1 time step = 12 minutes, and are run for 15,000 time steps. The patterning control coefficient (C_p), was found using the Reid et. al. image sequence and analyzing its length growth rate. Isometric control coefficient

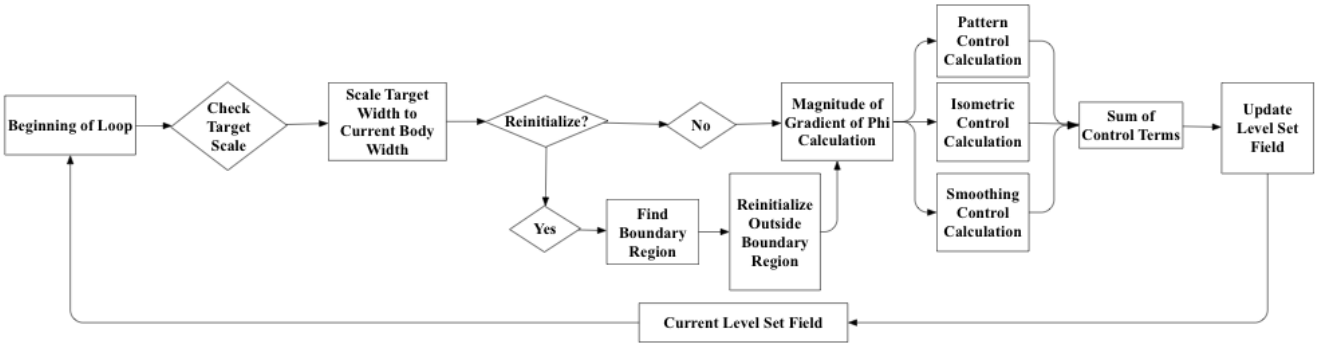

Figure 5: Implementation of primary simulation loop.

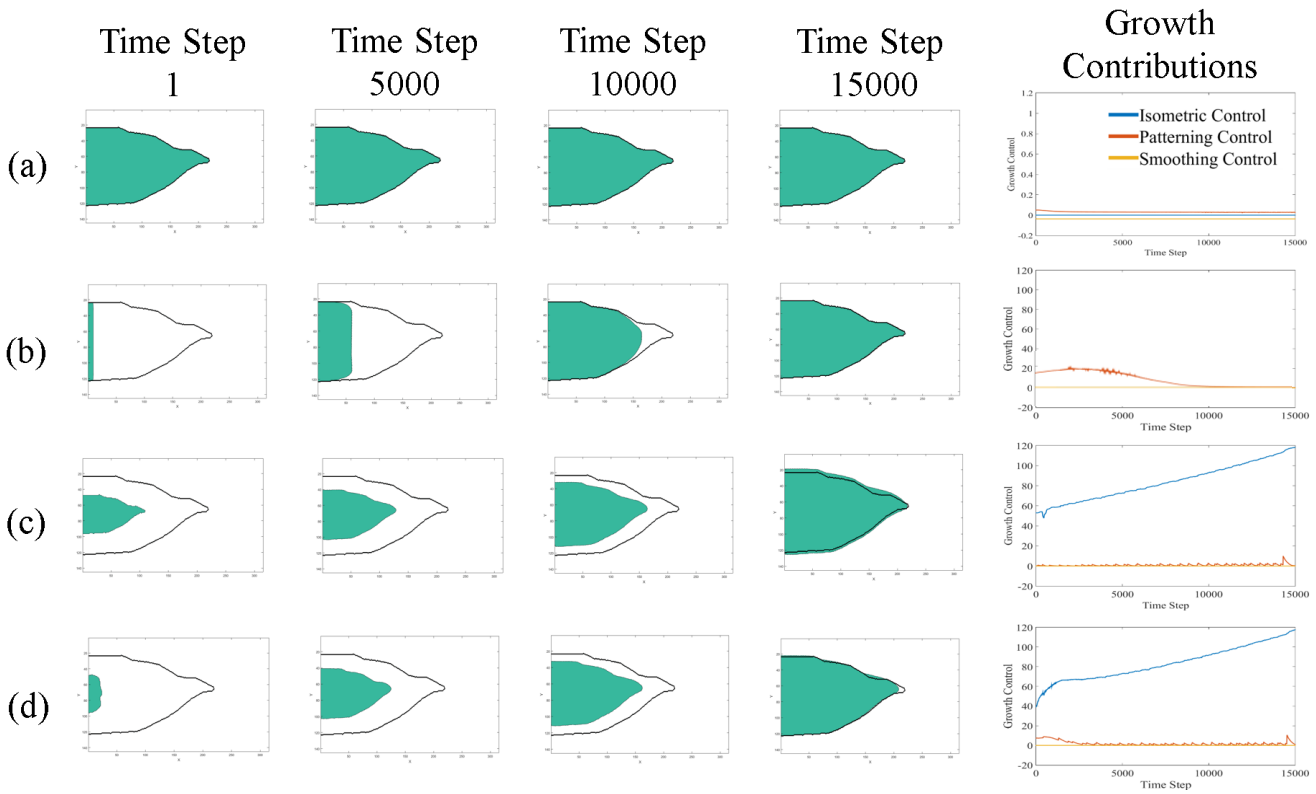

Figure 7: Verification tests: (a) No Growth, (b) Regeneration Following Amputation (c) Nominal Growth (d) Nominal Growth and Simultaneous Regeneration Following Amputation. The right most graph shows contributions of individual control terms to *F*, integrated over the simulation domain.

($C_{Gc,nom}$) was found using the normal table of *Xenopus laevis* stage series (Faber and Nieuwkoop 1967). The pixel area of the organism was evaluated from experimental images, between stages 40 and 52. Data were plotted and the value of the growth rate was determined by a linear fit of the data.

In analyzing the four test cases, it is useful to consider image sequences that illustrate the growth process. Figure 7 shows four image sequences, one for each test cases. At the end of each row, an additional plot shows growth contributions per time step for each term (P, I, and K). Each image sequence starts from the left; the green body is the current body shape, and the black outline is the final target reference. In the growth contributions plot (far right) the horizontal axis indicates time and the vertical axis indicates the growth contribution (for P, I, and K) integrated over the entire organism for each time step in units. Growth is measured in terms of grid cells, or pixels, that the organism fills. Hence the units of the vertical axis can be considered to be pixels per unit time. The area under each of the growth contribution curves can loosely be viewed as the overall contribution of material due to each growth contribution (P, I, and K) from the start of the simulation.

Case A: No Growth

The first test case looks at the stability of the patterning algorithm by considers a fully-grown tail where the surface of the organism is already at its reference location and where the nominal growth term is shut off ($C_{GC,nom} = 0$). One would expect there should be no change in body shape, and little to no contribution from any of the active control regimes, since the initial organism shape matches the reference contour. Indeed, the image sequence in Figure 7(a) shows qualitatively that the tail remains stationary. Growth contributions are tiny but nonzero (smaller than 0.1 pixel/time step, as shown in the growth contributions plot at the end of the row). Though nonzero, the growth contributions from patterning (positive) and smoothing (negative) are essentially balanced. The implication is that the smoothing term is continually active at a low level and that the patterning term compensates, such that the two remain in static equilibrium. The fact that the system reaches equilibrium indicates that the algorithm is in fact stable.

Case B: Regeneration Following Amputation

The second test case considers a simplified model of regeneration following amputation, with no nominal organism growth. The purpose of the test case is to examine the performance of the patterning control term. The amputation is performed digitally, with the tail being "cut" at the initial time to leave tissue only in the 10 leftmost grid cells of the image. For this simulation, nominal growth is again disabled ($C_{Gc,nom} = 0$). Under these conditions, we would expect the tail to return its nominal shape (pre-amputation), with tissue filling the reference map much as material might flow into a mold.

Figure 7(b) shows that by time step 15,000, the tail has in fact regenerated to its nominal shape and size. Note that, for Case B only, the patterning growth rate was reduced relative to its nominal value (to $C_p = 0.005$), in order to better visualize the growth process. As shown in the initial sequence, the corners created in the amputation persist through time step 5,000.

Together the smoothing term and the reference image (which inhibits patterning growth when the organism boundary reaches the reference boundary) introduce more curvature into the regenerating tail, as seen by time step 10,000. The smoothing term becomes more active as the tail becomes sharper, but eventually the patterning term overcomes the smoothing term to fill the pointed tip of the tail, as seen in time step 15,000.

The growth contribution plot shows that total patterning growth ramps up slowly to a peak around time step 4,000 before tapering toward zero approaching time step 10,000. The explanation is that initially the amputation boundary grows nearly straight (toward the right), such that the total patterning growth (which is proportional to the size of the amputation surface) is nearly constant with some slight rise due to the curvature appearing at the top and bottom corners of the amputated face. As the tail narrows, the surface area of the amputation face grows narrower and the amount of patterning growth falls quickly toward zero. Note that the scale of the growth contribution plot for Case B is zoomed out by 100 times relative to that of Case A, indicating much, much higher growth rates in Case B (as would be expected).

Case C: Nominal Growth

The third test case mimics nominal growth with no amputation or regeneration. In this example, the initial organism is set to the same shape as the initial organism in Case A, but scaled down in size by 50%. In concept, one would expect only isometric control would be necessary to grow the tail, even with patterning control active.

The simulation indicates that the organism shape is preserved during growth, as shown in Figure 7(c). The growth contributions plot for this row shows that the majority of all growth is generated by the isometric growth term. Though the patterning growth term is active, it remains essentially zero throughout the simulation, as expected. (The exception is a small spike near time step 15,000, triggered by a combination of the reinitialization process and by erosion due to smoothing). The final image of the sequence shows the simulated organism overgrows the reference contour slightly, as can be observed near the tip of the tail. This occurs largely because of the action of the smoothing term, which rounded the tail during otherwise isometric growth.

As a final note, it is worth observing that the organism growth rate increases slightly over time, as is evident from the growth contributions plot at the end of row (c) in Figure 7. The acceleration of growth over time matches the intent of equation (14), which was designed to keep the rate of cellular division constant, with the implication that the organisms total growth (pixels added per time step) should become faster as the organism becomes larger.

Case D: Nominal Growth and Regeneration

A final test case combines Cases B and C to provide a more realistic model for amputation, one in which patterning growth occurs in parallel with nominal growth. For this case, all three control terms are active simultaneously (with control parameters set to their nominal values).

The Case D simulation confirms that the patterning and isometric growth terms complement each other when they are both active, allowing the organism to change size and shape simultaneously. It is perhaps surprising to observe that the combined growth (Case D) image sequence much more closely resembles nominal growth (Case C) than regeneration (Case B). In fact, as early as time step 5000 of the image sequence, Case D and Case C appear qualitatively the same, even though the initial conditions (at time step 1) are entirely different. The similarity of the image sequences can be explained by examining the growth contributions plot, which shows that patterning growth term is most active early, approximately through time step 1000. In fact, the shape of the patterning growth curve for Case D is nearly identical to what was observed for Case B, but with a smaller peak amplitude and scaled to a shorter time scale (about five times faster completion of patterning as compared to Case B). The shortened duration of patterning growth is related to the choice of patterning growth coefficient C_p (which was reduced in Case B) and to the initial condition of Case D (which has half the width of the initial condition for Case B, such that the velocity-to-length ratio is increased in Case D).

At first glance, it appears that the growth contribution plot for Case D suggests some interaction between the isometric and patterning growth terms, since the isometric growth rate in Case D appears to dip for the first 1000 time steps as compared to Case C. This difference in the initial isometric growth can more simply be explained as a size effect, however, rather than an interaction. Since the total amount of isometric growth scales with the amount of material in the organism, and since the amount of simulated material is very low post amputation (in Case D), it should not be surprising that the volumetric growth rate is initially much lower in Case D than Case C.

Discussion

The verification tests described in the prior section, and in particular the Case D test, suggest that this simulation can provide a relevant model for simulation of *Xenopus* regeneration. In the Case D simulation, morphology is regenerated while the tail grows in size, a behavior seen in *Xenopus* regeneration. Importantly, the verification tests of the prior section also demonstrate that the simulation is stable and qualitatively well behaved. The patterning control switches off when the organism shape approaches the reference map (Case A). The isometric growth and volumetric terms perform as expected when active individually (Case B and Case C) and when active simultaneously (Case D). The smoothing control term was active in all cases, providing small adjustments to regularize shape (as visible in Case B in particular), but always resulting in a very small contribution to the overall growth of the simulated organism, so small that the contribution was only visible when magnifying the scale of the growth contribution plot (as in Case A).

The simulation does have limitations. First, the reinitialization process introduces slight irregularities, since reinitialization occurs only periodically (once every 20 time steps). The result is that the growth contribution plots can appear slightly choppy (as is visible in the saw tooth pattern for patterning growth in Case C and Case D). Reinitialization is also somewhat computationally intensive. As such, an alternative to reinitialization may be pursued in the future. Second, smoothing control effects make it difficult to generate sharp corners. Some modification to the smoothing control may be necessary in the future to allow sharp features to develop when desired (as in the tip of the simulated tail). Third, at small tail sizes, the discrete nature of the patterning control reference

map can introduce dithering when the reference map is rescaled. To mitigate this effect, we will consider alternate representations of the reference map in the future. Since, the current reference map is binary (with a one indicating a grid point inside the organism and a zero indicating a grid point outside), a floating point representation of the reference map would likely be helpful to reduce dithering that occurs when the reference map is scaled.

The intended application of our simulation tools is to examine control policies and sensing modalities that might be used during regenerative growth. Future studies will validate our simulation tools through direct comparison to biological studies of *Xenopus* tail regeneration. Also, we will augment our current simulations with new models of control and sensing with the goal of explaining biological observations about the impact of external factors (electrical, chemical, damage, etc.) on regenerative growth.

Conclusion

This algorithm creates a simplified abstraction of cell regeneration morphology, using level set methods and control regimes, that is a base module for a future framework to predictively link cell-level signaling to macroscopic patterning. This ultimate framework may provide insight into regeneration, cancer, and even birth defects. This algorithm reduces complex cellular interactions into body boundary movement using three control regimes – patterning control, isometric control, and smoothing control. Patterning control mimics regeneration at wound sites and acts on the body boundary. Isometric control mimics bulk growth of the organism with time, and smoothing control regularizes growth by reducing high curvature regions. Looking specifically at *Xenopus laevis* tail regeneration, this algorithm shows promise in predicting cell patterning on the macroscopic scale. Although this paper specifically discusses simulation of a *Xenopus* tail in two dimensions, the methodology is general enough to be applied to arbitrary morphologies in both two and three dimensions.

References

Bianconi, Eva, Allison Piovesan, Federica Facchin, Alina Beraudi, Raffaella Casadei, Flavia Frabetti, Lorenza Vitale, et al. 2013. "An Estimation of the Number of Cells in the Human Body." *Annals of Human Biology* 40 (6): 463–71. doi:10.3109/03014460.2013.807878.

Brakke, Kenneth A. 2015. *The Motion of a Surface by Its Mean Curvature. (MN-20)*. Princeton University Press.

Chernet, Brook T., Chris Fields, and Michael Levin. 2015. "Long-Range Gap Junctional Signaling Controls Oncogene-Mediated Tumorigenesis in Xenopus Laevis Embryos." *Biophysics* 5: 519. doi:10.3389/fphys.2014.00519.

C.S. Hogea, B.T. Murray, and J. A. Sethian. n.d. "Simulating Complex Tumor Dynamics from Avascular to Vascular Growth Using a General Level Set Method." *Journal of Mathmatical Biology*.

Evans, Lawrence C., and Joel Spruck. 1991. "Motion of Level Sets by Mean Curvature. I." *J. Differential Geometry* 33 (3): 635–81.

Faber, Jacob, and Pieter D. Nieuwkoop. 1967. *Normal Table of Xenopus Laevis (Daudin) : A Systematical and Chronological Survey of the Development from the Fertilized Egg till the End of Metamorphosis*. 2nd ed. Amsterdam : North-Holland Pub. Co.

Friston, Karl, Michael Levin, Biswa Sengupta, and Giovanni Pezzulo. 2015. "Knowing One's Place: A Free-Energy Approach to Pattern Regulation." *Journal of The Royal Society Interface* 12 (105): 20141383. doi:10.1098/rsif.2014.1383.

King, Ryan S., and Phillip A. Newmark. 2012. "The Cell Biology of Regeneration." *The Journal of Cell Biology* 196 (5): 553–62. doi:10.1083/jcb.201105099.

Kundu, Pijush K., Ira M. Cohen, and David R. Dowling Ph.D. 2011. *Fluid Mechanics*. 5th Edition. Academic Press.

Lobo, Daniel, Wendy S. Beane, and Michael Levin. 2012. "Modeling Planarian Regeneration: A Primer for Reverse-Engineering the Worm." *PLoS Comput Biol* 8 (4): e1002481. doi:10.1371/journal.pcbi.1002481.

Love, Nick R., Yaoyao Chen, Shoko Ishibashi, Paraskevi Kritsiligkou, Robert Lea, Yvette Koh, Jennifer L. Gallop, Karel Dorey, and Enrique Amaya. 2013. "Amputation-Induced Reactive Oxygen Species Are Required for Successful Xenopus Tadpole Tail Regeneration." *Nature Cell Biology* 15 (2): 222–28. doi:10.1038/ncb2659.

Osher, Stanley, and James A Sethian. 1988. "Fronts Propagating with Curvature-Dependent Speed: Algorithms Based on Hamilton-Jacobi Formulations." *Journal of Computational Physics* 79 (1): 12–49. doi:10.1016/0021-9991(88)90002-2.

Reid, Brian, Bing Song, and Min Zhao. 2009. "Electric Currents in Xenopus Tadpole Tail Regeneration." *Developmental Biology* 335 (1): 198–207. doi:10.1016/j.ydbio.2009.08.028.

Rejniak, Katarzyna A., and Alexander R. A. Anderson. 2011. "Hybrid Models of Tumor Growth." *Wiley Interdisciplinary Reviews: Systems Biology and Medicine* 3 (1): 115–25. doi:10.1002/wsbm.102.

Sethian, J. A. 1985. "Curvature and the Evolution of Fronts." *Communications in Mathematical Physics* 101 (4): 487–99. doi:10.1007/BF01210742.

Sethian, J.A. n.d. *Level Set Methods: Evolving Interfaces in Geometry, Fluid Mechanics, Computer Vision, and Materials Science*. Cambridge Monographs on Applied and Computational Mathematics.

Sethian, James. 1984. "Turbulent Combustion in Open and Closed Vessels." *Journal of Computational Physics* 54 (3): 425–56. doi:10.1016/0021-9991(84)90126-8.

Suzuki, Makoto, Nayuta Yakushiji, Yasuaki Nakada, Akira Satoh, Hiroyuki Ide, and Koji Tamura. 2006. "Limb Regeneration in *Xenopus Laevis* Froglet." *The Scientific World Journal* 6: 26–37. doi:10.1100/tsw.2006.325.

Walker, D.C., G. Hill, S.M. Wood, R.H. Smallwood, and J. Southgate. 2004. "Agent-Based Computational Modeling of Wounded Epithelial Cell Monolayers." *IEEE Transactions on NanoBioscience* 3 (3): 153–63. doi:10.1109/TNB.2004.833680.

Zhang, Ying, and Michael Levin. 2009. "Particle Tracking Model of Electrophoretic Morphogen Movement Reveals Stochastic Dynamics of Embryonic Gradient." *Developmental Dynamics*, no. 238: 1923–35.